Solar RRL
www.solar-rrl.com

Tuning Perovskite Crystal Growth Dynamics Using Additives on Textured Silicon Substrates

Mohamed A. A. Mahmoud, Oussama Er-Raji, Bhushan P. Kore, Martin Bivour, Patricia S. C. Schulze, Stefan W. Glunz, Andreas W. Bett, and Juliane Borchert*

Double-sided textured silicon solar cells with micrometer-sized pyramid structure are used as bottom cells in monolithic tandem structures to decrease reflection losses. As top cell material, frequently perovskites are used. In this work, various additives are investigated to enhance the perovskite absorber quality, as a top cell fabricated using the hybrid route. In the context of the hybrid route, it is found that urea or methylammonium chloride (MACl) can effectively increase the grain size and improve the absorber quality, while formamidinium chloride (FACl) cannot. With urea, the crystallization can be tuned without leaving any voids in the film (unlike MACl). However, when annealed at a high annealing temperature, the excessive crystal growth with urea causes non-conformal coating and high defect density. By adjusting the annealing conditions and additive concentration, the crystal growth of the perovskite top cell on the micrometer-sized silicon pyramids can be fine-tuned, ensuring that the perovskite layer conformally coated the pyramids. The use of additives not only improves crystallization but also enhances the conversion of the inorganics, particularly at the hole transport layer (HTL) interface. Moreover, this work contributes to a better understanding of perovskite crystallization dynamics and how to control it, especially on textured substrates.

1. Introduction

Perovskite solar cells have the advantage of a steep absorption edge, high defect tolerance, bandgap tunability, and cheap production methods. In a very short time, perovskite single-junction (SJ) solar cells went up from power conversion efficiency (PCE) of 3.8% to 26.1%, getting very close to the other established technologies that were developed for decades.[1] Perovskite was adapted in a dual-junction two-terminal monolithic form with silicon as a bottom cell in 2015 with PCE of 14.3% reaching the world record today of 33.9% to be the most efficient tandem solar cell of any technology.[1]

Most research laboratories are depositing perovskite layers by solution processing. However, applying this technique on top of textured silicon bottom cells with large pyramid size (micrometer range) results in low conformality.[2] The lack of conformality then causes shunt pathways, thus reducing the overall efficiency of such devices. As a result, more focus has been dedicated to polishing the bottom cells, which however results in higher production costs and poor light trapping as predicted by multiple simulation studies.[3–5] To overcome this issue, an alternative route of depositing the perovskite on textured silicon and simultaneously achieving high conformality was developed. The fabrication method is known as the hybrid route in which the perovskite is deposited in two steps (Figure S1, Supporting Information). The first step is the co-evaporation of the inorganic precursors, i.e., lead iodide (PbI_2) and cesium halide (Cs*X*, $X = I$ or Br), followed by the second step which is the wet-chemical deposition of the organohalide solutions, i.e., formamidinium iodide (FAI) and formamidinium bromide (FABr) dissolved in ethanol (EtOH). This route successfully produces perovskite films that fully cover the Si pyramids.[2,6] However, the resulting perovskite grain size is rather low, which lowers the bulk quality and limits the performance.[7–19] Therefore, tuning the crystallization of perovskite is necessary to obtain high-efficiency devices.

Many techniques have been implemented to increase the grain size of perovskite such as hot casting and changing the

M. A. A. Mahmoud, A. W. Bett
Insitute of Physics
University Freiburg
Freiburg 79104, Germany
E-mail: mohamed.mahmoud@ise.fraunhofer.de

The ORCID identification number(s) for the author(s) of this article can be found under https://doi.org/10.1002/solr.202400471.

DOI: 10.1002/solr.202400471

M. A. A. Mahmoud, O. Er-Raji, B. P. Kore, M. Bivour, P. S. C. Schulze, S. W. Glunz, A. W. Bett, J. Borchert
Division Photovoltaics (PV)
Fraunhofer Institute of Solar Energy Systems
Freiburg 79110, Germany

M. A. A. Mahmoud, O. Er-Raji, B. P. Kore, S. W. Glunz, J. Borchert
Freiburg Center for Interactive Materials and Bioinspired Technologies
University of Freiburg (FIT)
Freiburg 79110, Germany

O. Er-Raji, B. P. Kore, S. W. Glunz, J. Borchert
INATECH
University of Freiburg
Freiburg 79110, Germany

contact angle via different surface chemistry.[9,16,20] However, most of the techniques are applicable only to the solution processing techniques and the one-step deposition method. Therefore, this work aims to enhance the perovskite absorber quality using so-called "additives", to be added in the second step of the hybrid route deposition (i.e., wet-chemical step), as it is the most suitable technique for our system (hybrid route on textured substrates) and have been implemented by others.[18,19] Additives that are chloride based are the most common in literature and they are mainly targeting crystallization. It was shown that by adding, for example, methylammonium chloride (MACl), in $FAPbI_3$, the grain size increased up to six times and the efficiency increased substantially.[21] Another example of chloride-based additive is the recent record for the perovskite SJ solar cell with a PCE of 26.08%.[22] The working mechanism of all additives used for crystallization (including Cl-based additives) has been and is still debatable.[23–25] In addition to Cl-based additives, Lewis base additives have been used. Based on literature, they can enlarge the perovskite grain size to more than 2 μm.[26–29]

In this work, we investigate the crystallization dynamics during the hybrid route including as well the influence of additives. We investigate Cl-based additives namely MACl and FACl as well as a Lewis base additive namely urea in the context of the hybrid route deposition on planar and textured substrates. We find similar effects for the additives on the perovskite grain size on planar and textured substrates. MACl or urea as an additive significantly increases the grain size, while FACl-modified samples show comparable grain size to pristine films. We also show that annealing temperature and time plays a vital role on the conformality of the perovskite films on the micrometer-sized textured Si substrates and for the complete chemical reaction between the scaffold (inorganics) and the organic molecules (from the wet-chemical step). Finally, we investigate the phase formation of the perovskite film at the different stages of the hybrid route to better understand the chemical reaction between the different steps of the hybrid route as well as the successful crystallization tuning which happened using only certain additives with certain concentrations.

2. Influence of Additives on Perovskite Crystallization

First, we investigate the effects of the different additives on planar Si substrates. Figure S2, Supporting Information, shows the effect of incorporating MACl on perovskite crystallization deposited on planar substrates. By adding MACl, one can see larger grain sizes than the pristine: the higher the concentration of incorporated MACl, the larger the mean grain size (Figure S3, Supporting Information). However, the SJ solar cells made with MACl as an additive were shunted compared to the pristine (Figure S4, Supporting Information). To understand the origin of the shunt behaviour, we took a deeper look at the scanning electron microscope (SEM) images. Figure S5, Supporting Information, shows voids in the morphology of the sample with incorporated MACl. These voids formed pathways for current to escape instead of getting collected (i.e., shunts). In addition, we characterized the solar cells by dark lock-in thermography (DLIT) to detect possible shunts (Figure S28, Supporting Information). Only in one of the three cases, we observed a distinct shunt. The other two images show only noise, indicating that there is no single distinct shunt. More likely, the shunts are homogeneously distributed. Since the images are captured through the glass side and glass partially blocks IR radiation, the homogeneously distributed signal is then too low to be distinguished from noise. While this does not prove the presence of nano-voids, it shows that for two of the three images no other shunt path is present. Note that for higher excitation voltages, we would have probably been able to see a homogeneous signal along the whole cell area even through the glass but exciting the cell way beyond its open-circuit voltage (V_{OC}) has the potential to damage the cell itself and generate further shunts.

Here, it is worth mentioning that after the hybrid route deposition, the samples were subjected to an annealing temperature of 150 °C for 25 min. The temperature and time were optimized within a previous study that showed the higher the annealing temperature and annealing time for samples without additives (pristine), the larger the grain size.[30] Here we applied the optimized annealing temperature and time. To understand the origin of these voids, we did an energy-dispersive X-ray (EDX) analysis (Figure S6, Supporting Information). The samples with added MACl showed no chlorine. This suggests the high volatility of MACl, which escaped the film and left voids behind. The high volatility of MACl is also well reported in the literature.[31,32] We supported the EDX results with X-ray photoelectron spectroscopy (XPS) data, which also does not show any chlorine intensity (Figure S10 and S11, Supporting Information).

In addition to MACl, we also investigated FACl as another Cl-based additive. Figure S7, Supporting Information, shows the effect of the different concentrations of FACl on the morphology of the perovskite. The grain size is very comparable to the pristine. X-ray diffraction (XRD) measurements also support the same results (Figure S7, Supporting Information): the same full width at half maximum (FWHM) was obtained for the different concentrations of FACl as the pristine, which indicates the same crystal size. The findings suggest that FACl does not tune the crystallization in the context of the hybrid route. In addition, the morphology of the FACl-treated perovskites with different concentrations did not feature voids. To investigate if the chlorine also left the film or not, we carried out EDX analysis. The analysis indicates the existence of a chlorine peak for the FACl sample (unlike MACl) as shown in Figure S6, Supporting Information. This suggests that FACl is less volatile than MACl and chlorine did not leave the film (unlike MACl). We also measured XPS to confirm the results. The XPS shows the existence of chlorine in the whole bulk for the FACl even after annealing for 25 min at 150 °C (Figure S11, Supporting Information). The results confirm that the volatility of the FACl is lower than the MACl and to a large extent, this can explain the voids observed in the film with MACl.

The third investigated additive is urea. Figure S8, Supporting Information, shows the effect of the different concentrations of incorporated urea on perovskite crystallization. Urea improved the grain size substantially. One can see the increase in the grain size with an increase in urea concentration until reaching saturation (a similar grain size–concentration dependence as MACl) (Figure S9, Supporting Information). To measure the optoelectronic quality of the absorbers, steady-state and transient PL measurements were done. The urea-modified samples show much higher radiative recombination and a higher carrier

lifetime (Figure S8, Supporting Information). The high PL suggests that the non-radiative recombination was suppressed: this can be due to the lower defect density originating from the lower grain boundaries in the urea-based samples. The findings suggest that the lower density of grain boundaries also translates to a higher carrier lifetime for the excited charge carriers.

After we investigated the effects of additives on planar substrates, we carried out the same experiments on top of micrometer-sized textured Si substrates. Here, the main difference between planar and textured substrates is that the scaffold (inorganics) is of a higher thickness (more detail in experimental methods). The effect of the different additives on the morphology of the perovskite absorber on top of textured substrates is shown in **Figure 1**. The results for textured substrates are very similar to those on planar substrates: pristine and FACl show comparable results with a lot of grain boundaries, while MACl and urea show lower grain boundaries. One can also see that with the fewer grain sizes (pristine and FACl), the perovskite conformally follows the textured substrates while in the case of the larger grain sizes (especially annealed at high temperature), one can see that the absorber layer was more flattened. The SEM top-view scans, as shown in Figure S12, Supporting Information, show voids very clearly everywhere in the MACl-modified sample (an enlarged image only with the MACl-modified sample can be found in Figure S13, Supporting Information). These results show the reproducibility of the effect of the different additives on the crystallization of perovskite as it is comparable to the results we obtained on planar substrates. XRD results support the crystallization tuning with MACl and urea compared to FACl and pristine. One of the issues we were facing with the pristine absorber in tandem devices is the unconverted lead iodide (12.7°) as shown in the XRD results (and SEM in Figure S19, Supporting Information). The thickness of the scaffold was adapted from 300 to 550 nm when we moved from SJ (planar substrates) to tandem devices (to ensure full coverage of pyramids as well as current matching). However, with all additives used, one can see that the lead iodide was not detected as strongly as for the pristine perovskite films.

The optoelectronic characterization shows that the lifetime of the excited charge carriers increases as the grain size increases (Figure S14, Supporting Information). Films with added FACl showed a very comparable lifetime as the pristine, while higher carrier lifetimes were obtained for the films with larger grain sizes with MACl or urea as the additives. All the previous results suggest that the most promising additive for crystallization tuning among the additives mentioned earlier is urea as it improved the crystallization and did not show any voids as in the case of MACl. Therefore, urea was used to optimize the grain size and was implemented in a monolithic tandem device. However, when we made tandem devices using various concentrations of urea, the result was shunted cells (Figure S15, Supporting Information). The data suggests shunts in the top cell of the tandem due to the very low V_{OC}. We suspected the almost bare pyramids contributed to the shunted behaviour. One can see these bare pyramids in Figure 1 (and in Figure S16, Supporting Information, with red arrows), especially for the MACl- and urea-modified cells which showed non-conformal deposition by not taking the shape of the textured silicon. We suspected the excessive grain growth created this non-conformal coating as well as defects.

In the box plot in Figure S15, Supporting Information, one can see 0 h and higher hours: 0 h indicates first-time measurement, while, for example, 3 h indicates 3 h of leaving the cells under 1 sun and in open-circuit conditions and then measure the current-voltage (jV) curve. One can notice a phenomenon for the pristine tandem cells that does not exist with the urea tandem cells: the light-soaking effect. First-time jV measurements show very poor performance for pristine devices and after light soaking, the performance improves dramatically. This is

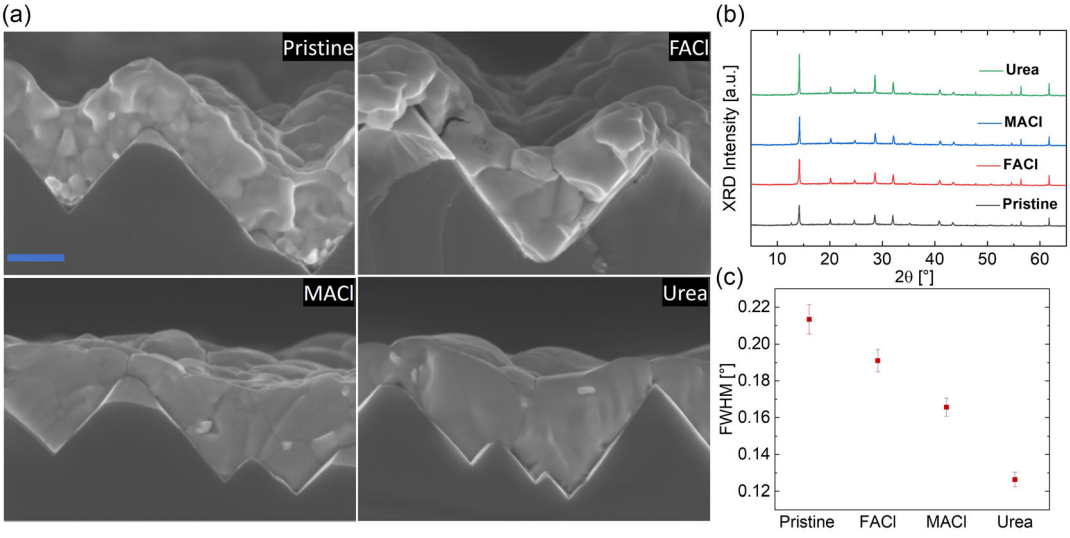

Figure 1. a) Cross-section SEM images of perovskite films without (pristine) and with the incorporation of different additives (7 mg mL^{-1}). Larger grain sizes are seen with MACl and urea, while FACl is comparable to the pristine (the blue scale bar is 600 nm). b) XRD of the perovskite films without and with the different additives after annealing for 15 mins at 150 °C. c) FWHM at the perovskite peak (100) of $2\theta = 14.1°$. Urea and MACl have the highest impact on the crystallite size.

attributed to the higher unconverted lead iodide at the interface (as shown in Figure S19, Supporting Information). One might argue that the photodecomposition of lead iodide might have happened under light illumination. Indeed this can be true, however, it needs to be accompanied by temperatures higher than room temperature.[33] As the measurements were done at standard temperature, i.e., 25 °C, this weakens such an argument. The reference cells needed light soaking for a long duration to reach the stabilized efficiency (more details can be found in ref. [34] and therefore the same measurement routine was applied to the urea-modified cells for comparison and also for testing its stability.

3. Optimizing Conformal Layer of High-Quality Perovskite on Textured Silicon Substrates

We tried different annealing strategies for the urea-modified cells to improve the non-conformal top cell growth. The results, interestingly, show that 1 min of annealing at 150 °C gives the same crystallite size as 15 mins (**Figure 2**). By comparing the cross-section images of SEM (Figure S16, Supporting Information), one can see that the low annealing time strategy leads to the formation of a perovskite absorber which takes the shape of the texture while it is obvious here for example when the annealing time was 10 min, the conformality is lower (the film appears to flow down into the valleys of the texture and does not follow the shape of the texture). This was directly reflected in the shunted cells we got when we made tandem devices for the high annealing time samples (**Figure 3**). The fact that very thin perovskite layers also result in shunted behavior (and not only bare pyramids) is shown in Figure S27, Supporting Information, where we deposited a 300 nm perovskite layer. Therefore thicker conformal layers of perovskite are necessary to avoid shunts. In contrast, the cells with low annealing time showed the highest performance due to a conformal growth avoiding severely shunted behaviour (one can see this clearly also from the voltage). However, a limitation in the fill factor (*FF*) is shown due to high R_S as the reaction was not complete and lead iodide remnants reside at the interface. This shows that a certain amount of energy is needed for the reaction to happen, but the annealing temperature also plays a major role in controlling the crystal growth as will be shown later.

After the aforementioned investigations, our goal was to control the dynamics of the crystal growth to get high conformality over the pyramids (by doing so the shunt resistance R_P is maximized) and at the same time to have enough reaction time for the full conversion of lead iodide especially at the interface with the hole-transport layer (HTL) (by doing so the series resistance R_S is minimized). We concluded from the previous results that this can happen by giving the system enough energy for the full reaction to happen and at the same time a lower heat transfer rate to control the crystallization growth dynamics on textured substrates. To achieve both goals, we decreased the annealing temperature and increased the annealing time. We tested different annealing temperatures for urea-modified perovskite (**Figure 4**). Interestingly, we found that the crystallite size is temperature independent for the tested temperature range for the urea-modified samples. The thermal energy budget needed for crystallization tuning with urea, based on the various annealing temperature and time tracking experiments we did, is very low. Figure S21, Supporting Information, shows that the PL intensity was the highest for the lowest annealing temperature. The trend suggests that the lower temperature annealing reduces defects caused by excessive grain growth. At this point, we concluded that high annealing temperature and time cause a lot of defects and non-conformality. XRD and SEM suggest that one can go to a lower annealing temperature without any limitations to the crystalline quality.

As 100 °C showed the same improved crystallinity as 175 °C, we decided to anneal at 100 °C and vary as well the annealing time. The previous results were done at 15 min annealing. Here we tried various annealing times (**Figure 5**). Interestingly, with only 1 min

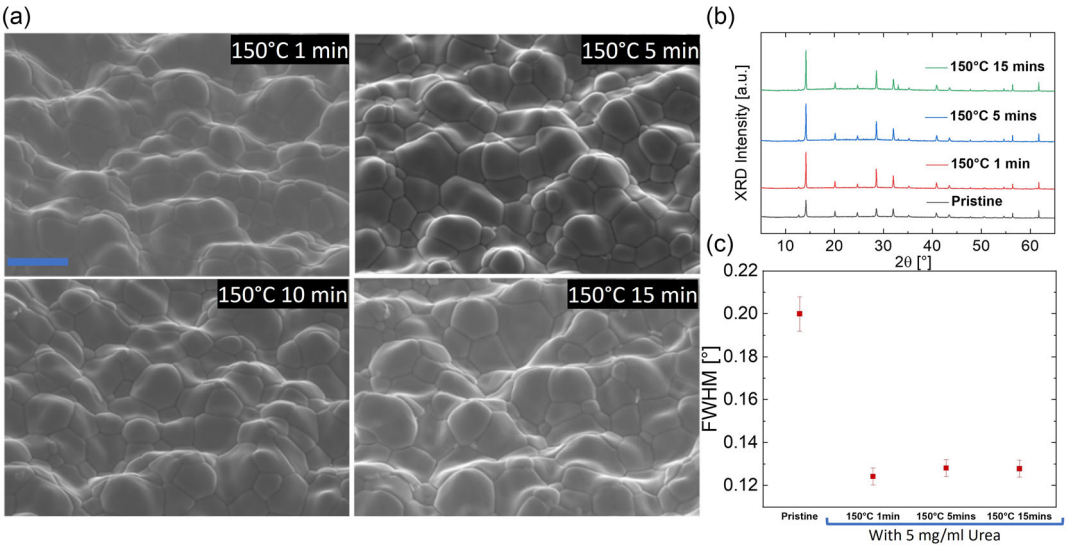

Figure 2. a) Top-view SEM images of perovskite films with the incorporation of 5 mg mL^{-1} urea at 150 °C for different annealing times (the blue scale bar is 2 µm). b) XRD of the perovskite films with urea after annealing at 150 °C for different annealing times. c) FWHM at the perovskite peak (100) of $2\theta = 14.1°$. The same FWHM for urea-modified samples was obtained with different annealing times.

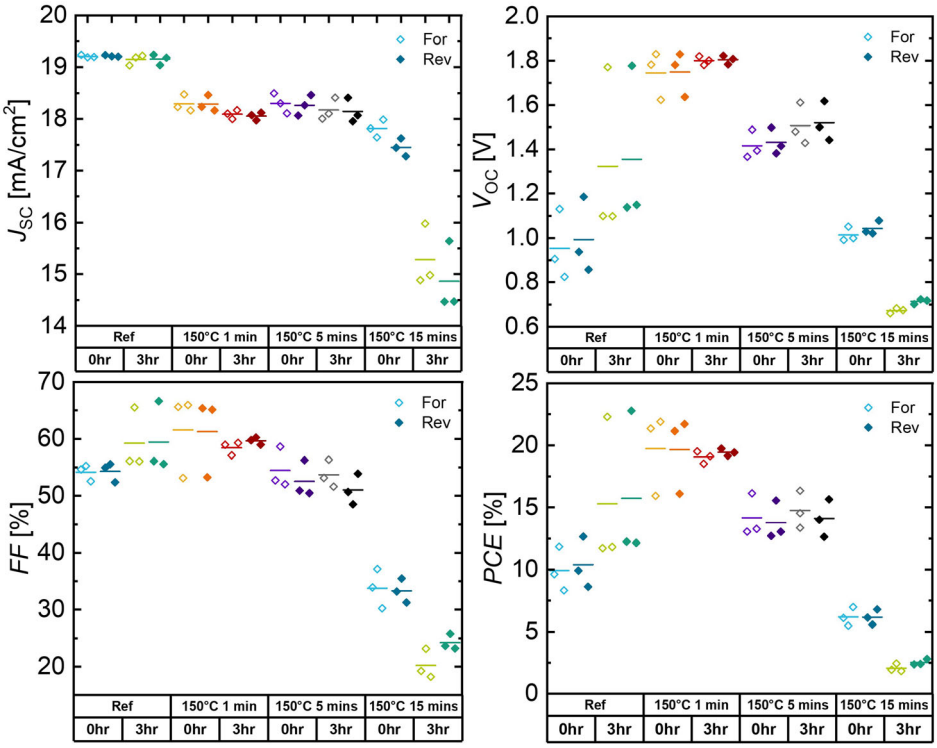

Figure 3. Plots of j_{SC}, V_{OC}, FF, and PCE of the perovskite–silicon tandem solar cells with incorporated 5 mg mL^{-1} of urea annealed at 150 °C annealed for 1, 5, and 15 min in comparison to pristine devices. The bottom bar indicates the time of illumination. 0 h indicates first-time measurement and 3 h indicates measuring after 3 h under illumination at open-circuit conditions.

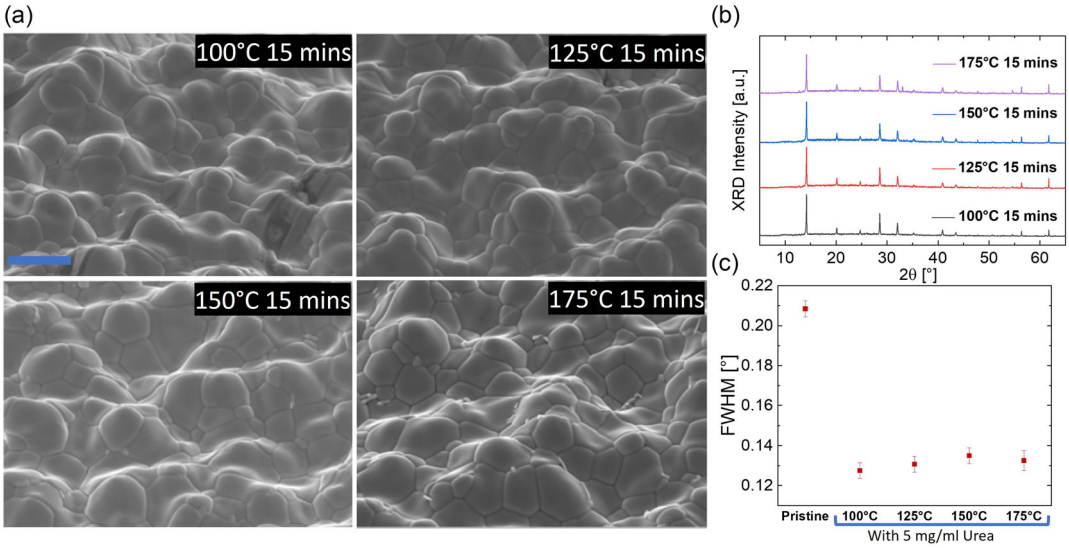

Figure 4. a) Top-view SEM images of perovskite films with the incorporation of 5 mg mL^{-1} urea after annealing for 15 min at different annealing temperatures. Same apparent grain sizes with different annealing temperatures. At 175 °C, remnants of lead iodide started to appear as well as cracks (more in Figure S17, Supporting Information) (the blue scale bar is 2 μm). b) XRD of the perovskite films with urea after annealing at different annealing temperatures for 15 min. c) FWHM at the perovskite peak (100) of $2\theta = 14.1°$. The same FWHM for urea-modified samples was obtained with the different annealing temperatures.

annealing at 100 °C, a similar grain size is obtained to that with 15 min. However, a high density of unconverted lead iodide residuals were found at the valleys, which is undoubtedly detrimental for the PCE due to the increased R_S. Indeed this was the case when we made tandems out of these cells (**Figure 6**). The 1 min annealing samples show the lowest *FF* due to the high R_S. With longer

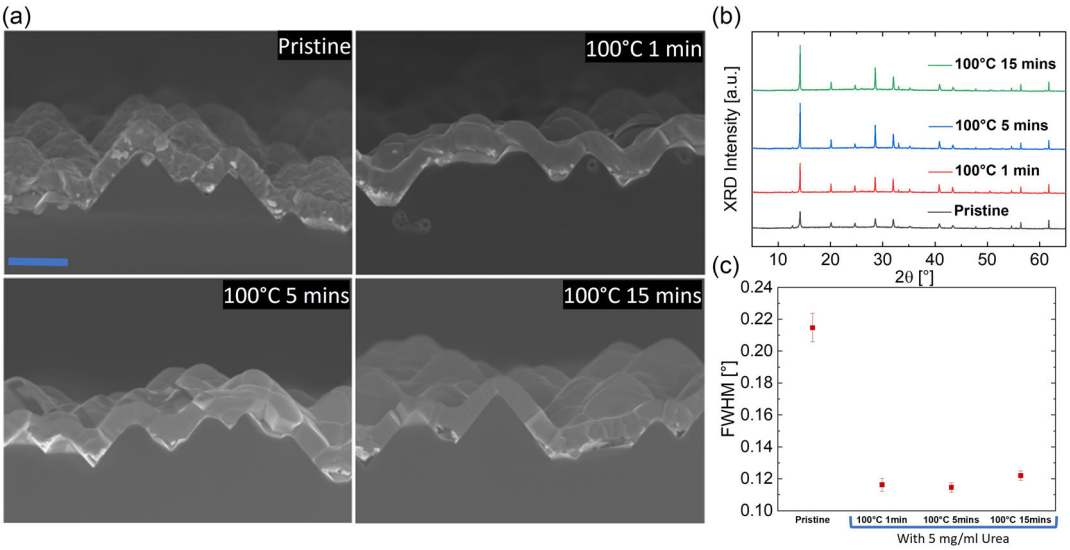

Figure 5. a) Cross-section SEM images of perovskite films without any additive (pristine) annealed at 150 °C for 25 mins (reference) and perovskite films with the incorporation of 5 mg mL^{-1} urea annealed at 100 °C for different annealing times (the blue scale bar is 2 µm). b) XRD of perovskite films without any additive (pristine) annealed at 150 °C for 25 mins and perovskite films with the incorporation of 5 mg mL^{-1} urea annealed at 100 °C for different annealing times. c) FWHM at the perovskite peak (100) of $2\theta = 14.1°$.

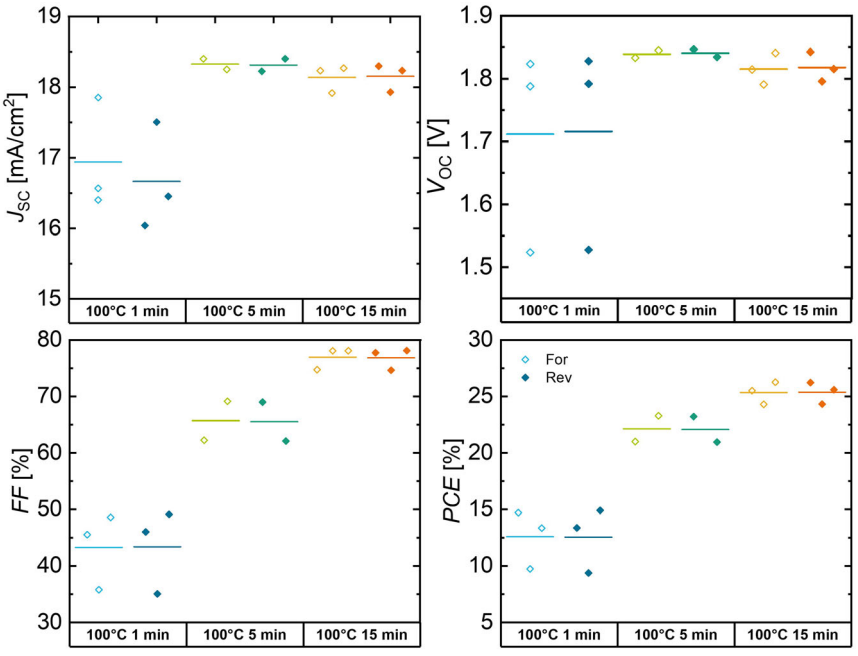

Figure 6. Plots of j_{SC}, V_{OC}, FF, and PCE of the perovskite–silicon tandem solar cells with incorporated 5 mg mL^{-1} of urea annealed at 100 °C for 1, 5, and 15 min. With higher annealing time, less inorganics reside at the interface with the HTL improving mainly FF and so too PCE. A comparison to pristine and stability testing can be found in Figure S23, Supporting Information.

annealing time, the R_S is reduced due to the full conversion of the lead iodide, which translates to higher *FF*. Here, one can notice that we obtained the energy from the top cell at all time variations—unlike annealing at higher temperature (150 °C)—which suggests conformal growth. One can see the conformal growth clearly in Figure 5. Figure S20, Supporting Information, shows a top-view image. It shows clearly the improvement in the grain size with urea as well as a new feature which is stripes, especially at 100 °C for 5 and 15 min (more details can be found in ref. [34]).

In the jV plots (Figure 3, and S15, Supporting Information), one can also see the trend in the short-circuit current density (j_{SC}): the higher the grain sizes, the lower the j_{SC} and this

can be explained by the higher reflection losses due to the flattened morphology with bigger grains (Figure S24, Supporting Information). One can also see this clearly in Figure 1, S12, and S20, Supporting Information: the peaks and valleys are more apparent with the pristine. In general, what is limiting the performance the most is the j_{SC} even for the pristine devices. One of the reasons was due to the high shadowing effect due to the increased silver area on top. We therefore designed an improved silver mask with less shadowing and this resulted in an improvement in the j_{SC} and an efficiency of 28.5% was measured (**Figure 7**).

4. Hybrid Route Phase Analysis and Crystallization Dynamics

To understand the film formation and the reason behind the successful crystallization tuning with MACl and urea in contrast to FACl and pristine devices, we investigated the film formation at different stages. Firstly, we investigated the phase composition of the film before spin coating (i.e., directly after the co-evaporation of the inorganic precursors, referred to as scaffold). Then, we checked the phase composition directly after the spin coating of the organohalides (before annealing) with and without the different additives (**Figure 8** and S22, Supporting Information, respectively). After the first step, which is co-evaporation of the inorganics, the lead iodide peak (001) at 2θ of 12.7° emerges. After the second step of the hybrid route, which is the spin coating of the organohalides on the scaffold, one can notice the emergence of a second peak around 2θ of 10° (which might correspond to the orthorhombic perovskite phase of $CsPbI_3$). This shows that the annealing step is essential as it helps in the nucleation and crystal growth of the α-perovskite phase and the full conversion of the scaffold as shown previously. One can think of the hybrid route then as a non-spontaneous chemical reaction at room temperature (to reach the α phase). For the chemical reaction to take place and produce the photoactive cubic perovskite α phase, one has to give the system energy to overcome the activation energy barrier, for example, by annealing or using certain additives with certain concentrations as will be discussed later (Equation (1)).

$$CsI + PbI_2 + FAI + FABr \xrightarrow{\text{annealing/certain additives}} \alpha FA_xCs_{1-x}Pb(I_xBr_{1-x})_3 \quad (1)$$

By comparing the film formation between the reference and the additive-modified films (still before heat treatment), we found an identical film formation—identical to reference—for the 3 mg mL^{-1} concentration of MACl and FACl (Figure S22, Supporting Information). However, by increasing the concentration from 3 to 7 mg mL^{-1}, the sample with MACl showed already α-phase perovskite formation at room temperature while the sample with FACl showed similar results to the low concentrations and the reference. And, 3 mg mL^{-1} of urea was enough to create a new phase of the photoactive cubic α-perovskite phase at room temperature, unlike MACl and FACl. This can be interpreted as follows: primary nucleation of perovskite happened for the 7 mg mL^{-1} MACl and 3 and 7 mg mL^{-1} urea samples before annealing treatment. Upon annealing, the crystal growth rate outruns the secondary nucleation rate (suppressing it) resulting in big grain sizes for the primary nuclei. This can explain as well the high standard deviation for the grain size observed in Figure S3 and S9, Supporting Information, for the samples with MACl or urea. The small grain sizes in that plot can be attributed to the growth of the secondary nuclei while the big grain sizes originate from the primary ones. Pristine films and films with FACl had only their primary nucleation upon annealing and therefore the suppression to new nucleation sites we have seen with the urea and MACl did not take place. To further prove that low concentrations of MACl ($\leq$3 mg mL^{-1}) cannot successfully tune the perovskite crystallization with the hybrid route, an experiment with 2 mg mL^{-1} was carried out. Figure S18, Supporting Information, shows the XRD of 2 mg mL^{-1} incorporated MACl annealed at 150 °C for 25 min. The FWHM did not decrease with 2 mg mL^{-1} MACl in comparison to the pristine sample, thereby supporting the proposed working mechanism.

By taking a closer look at the XRD of the samples with urea (Figure S22, Supporting Information), one will find a peak at 11.6° for urea-modified samples which corresponds to the formation of the δ phase of perovskite. This supports that at room temperature, after the interaction of the organic compound urea with the other compounds, the coexistence of the α and δ phases of

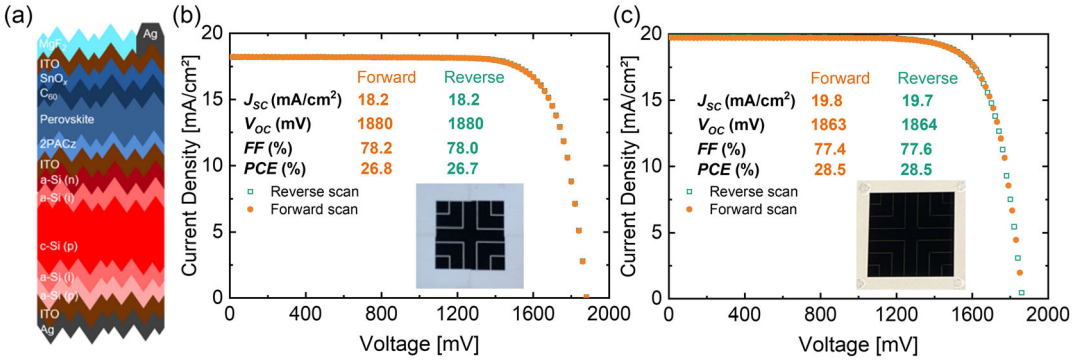

Figure 7. A comparison in the jV parameters between two cells (active area: 1 cm^2) with a) the cell structure using b) silver mask with high shadowing effect resulting from thick finger width (100 µm) and c) an optimized silver mask design with less shadowing effect due to thinner finger width (25 µm) that enabled higher short-circuit current density, j_{SC}. Design of the mask can be found in Figure S25, Supporting Information. The two cells had urea as an additive with concentration of 5 mg mL^{-1} and was annealed at 100 °C for 15 min.

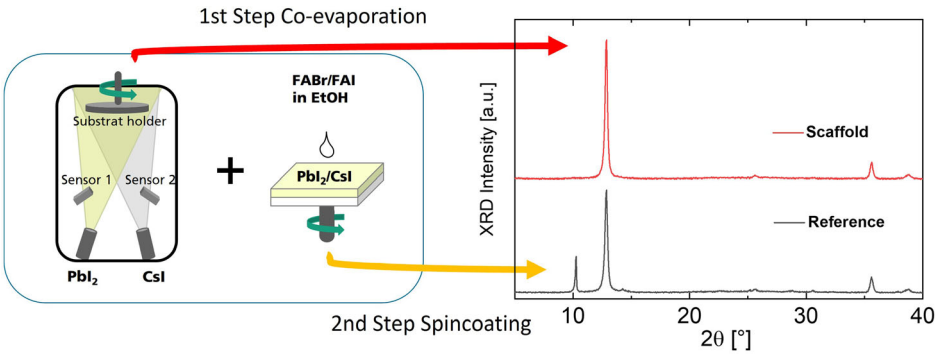

Figure 8. Phases during film formation at different stages of hybrid route before annealing (without additives). Scaffold refers to the film after the co-evaporation of the inorganics. Reference refers to the film after adding the organohalides in the second step on the scaffold.

perovskite emerges. The transition from the δ to the α phase happened upon annealing very fast and at low annealing temperatures as supported by the previous subsections. By comparing the different incorporated urea concentrations with the reference, the lead iodide peak did not exist in the urea samples. This might support the interaction between urea as a Lewis base with lead iodide by donating electrons to the uncoordinated Pb^{2+} ions to form a Lewis adduct as we also see the formation of new phases for the samples with urea (unlike with MACl, which did not show any new phase except for the perovskite α phase at only high concentrations).

From the aforementioned analysis, we can conclude the following: the formation of the photoactive α-cubic-perovskite phase at room temperature before the annealing treatment is essential to tune the crystallization of perovskite with the hybrid method. An amount of 3 mg mL^{-1} of urea was enough to create a new phase of the photoactive cubic α-perovskite phase at room temperature, which points toward primary nucleation taking place. Based on the proposed working principle, this can explain why at such low concentrations we were able to see an increase in the grain size of the perovskite film (Figure S8, Supporting Information). This was not the case for MACl. Crystallization tuning was achieved using MACl (only at high concentrations) and urea (at low and high concentrations) due to the formation of the α-perovskite phase at room temperature before annealing: primary nucleation. Upon annealing, the crystal growth rate is higher than the secondary nucleation rate creating bigger grain sizes for the primary nuclei. The fact that crystal growth rate is higher than nucleation rate at elevated temperature is a classical well-known phenomena for many other materials and is based on classical nucleation theory.[35–39] In previous work[30] as well as this work, we found out that perovskite exhibits the same crystallization dynamics.

5. Conclusion

In this work, we have tested different additives to increase the grain size of perovskite films with different annealing strategies and on different substrate architectures. The findings suggest that additives can be effective in increasing the grain size in the context of the hybrid route under certain conditions such as certain annealing temperatures, additive concentrations, and annealing times. The findings suggest that the two-step heterogenous reaction using the hybrid route is a non-spontaneous chemical reaction and a certain amount of energy is needed to overcome the activation energy barrier. However, to control conformal coating over the pyramids, a low annealing temperature is needed and at the same time, enough energy needs to be delivered to the system for the full reaction to take place. This means that a low annealing temperature scenario needs a longer time for the full reaction to take place. We found that urea can increase perovskite grain size at any given concentration; while MACl can increase the grain size after reaching certain concentrations. FACl as an additive was also tried out and it is the least effective to increase the grain size: as it can only enhance the lead iodide conversion as revealed by XRD measurements. Furthermore, the results suggest that larger grain sizes improve the performance of the device mainly due to improved *FF* and V_{OC}. The improved *FF* can be explained by the reduction of the grain boundaries, which enhances the charge transport and lifetime of the excited charge carriers as proven by transient PL measurements. The enhanced V_{OC} comes from the suppression of the non-radiative recombination as proven by the higher PL signal with larger grain sizes compared to smaller ones. We found that the perovskite crystallization with urea as an additive happens extremely fast during annealing; while full conversion of lead iodide takes time. We noticed at high annealing temperatures, the formed films lack conformality and the silicon pyramids become non-fully covered resulting in shunted cells. The annealing temperature was reduced to 100 °C and the crystal growth dynamics were then better controlled improving the conformality of the top cell on top of the textured bottom cell without any loss to the grain size. With low annealing temperatures, not only the V_{OC} improved but also the *FF*, as we were able to anneal for a longer time—without any loss of conformal coating—and by doing so the lead iodide conversion, was improved. The improved *FF*, we obtained, is mainly due to two factors: first, the good control of the crystal growth of the perovskite absorber over the bottom silicon cell creates a conformal layer without bare pyramids, thereby increasing the shunt resistance R_P and second, the conversion of most of the lead iodide at the interface with the HTL decreases the series resistance R_S.

Supporting Information

Supporting Information is available from the Wiley Online Library or from the author.

Acknowledgements

The authors would like to thank Karin Zimmermann and Henning Nagel for silicon bottom solar cell processing, Jutta Zielonka for her support with SEM measurements, Angelika Schmidt for XPS measurements, K. Aborov for EQE and reflection measurements, Alexander J. Bett for fruitful discussion regarding EQE data, Oliver Fischer for DLIT measurements and for the fruitful discussion to interpret the measurements, Konrad Fischer for the design of silver masks and technical support, and Jacob Myers for technical support. This work was funded by the Fraunhofer LIGHTHOUSE PROJECT MaNiTU, the German Federal Ministry for Economic Affairs and Climate Action under contract no. 03EE1086A (PrEsto), as well as the Vector Stiftung.

Conflict of Interest

The authors declare no conflict of interest.

Author Contributions

Mohamed A. A. Mahmoud: Conceptualization (lead); Data Curation (lead); Formal Analysis (lead); Investigation (lead); Methodology (lead); and Writing—Original Draft (lead). **Oussama Er-Raji**: Formal Analysis (supporting); Methodology (supporting); Supervision (lead); and Writing—Review and Editing (supporting). **Bhushan P. Kore**: Writing—Review and Editing (supporting). **Martin Bivour**: Resources (supporting). **Patricia S. C. Schulze**: Writing—Review and Editing (supporting). **Stefan W. Glunz**: Resources (supporting). **Andreas W. Bett**: Supervision (supporting) and Writing—Review and Editing (supporting). **Juliane Borchert**: Supervision (supporting) and Writing—Review and Editing (supporting).

Data Availability Statement

The data that support the findings of this study are available from the corresponding author upon reasonable request.

Keywords

additives, crystallization, hybrid route, perovskite-silicon tandem solar cells

Received: June 28, 2024
Revised: August 28, 2024
Published online: October 24, 2024

[1] Best Research-Cell Efficiency Chart, Photovoltaic Research, NREL, https://www.nrel.gov/pv/cell-efficiency.html (accessed: April 2024).
[2] P. S. C. Schulze, K. Wienands, A. J. Bett, S. Rafizadeh, L. E. Mundt, L. Cojocaru, M. Hermle, S. W. Glunz, H. Hillebrecht, J. C. Goldschmidt, *Thin Solid Films* **2020**, *704*, 137970.
[3] K. Jäger, J. Sutter, M. Hammerschmidt, P.-I. Schneider, C. Becker, *Nanophotonics* **2021**, *10*, 1991.
[4] F. Sahli, *Doctoral Thesis*, **2020**, https://infoscience.epfl.ch/entities/publication/bda35394-063c-4ba6-8212-b39cd128043f.
[5] F. Gota, R. Schmager, A. Farag, U. W. Paetzold, *Opt. Express* **2022**, *30*, 14172.
[6] F. Sahli, J. Werner, B. A. Kamino, M. Bräuninger, R. Monnard, B. Paviet-Salomon, L. Barraud, L. Ding, J. J. Diaz Leon, D. Sacchetto, G. Cattaneo, M. Despeisse, M. Boccard, S. Nicolay, Q. Jeangros, B. Niesen, C. Ballif, *Nat. Mater.* **2018**, *17*, 820.
[7] Z. Guo, A. K. Jena, G. M. Kim, T. Miyasaka, *Energy Environ. Sci.* **2022**, *15*, 3171.
[8] C.-M. Hsieh, Y.-S. Liao, Y.-R. Lin, C.-P. Chen, C.-M. Tsai, E. Wei-Guang Diau, S.-C. Chuang, *RSC Adv.* **2018**, *8*, 19610.
[9] K. Liao, C. Li, L. Xie, Y. Yuan, S. Wang, Z. Cao, L. Ding, F. Hao, *Nano-Micro Lett.* **2020**, *12*, 1.
[10] D. Zheng, T. Pauporté, *J. Mater. Chem. A* **2021**, *9*, 17801.
[11] L. Mcgovern, I. Koschany, G. Grimaldi, L. A. Muscarella, B. Ehrler, *J. Phys. Chem. Lett.* **2021**, *12*, 2423.
[12] X. Xu, Y. Sun, D. He, Z. Liang, G. Liu, S. Xu, Z. Li, L. Zhu, X. Pan, *J. Mater. Chem. C* **2021**, *9*, 208.
[13] J. Kumar, P. Srivastava, M. Bag, *Front. Chem.* **2022**, *10*, 330.
[14] Z. Xue, S. Wang, J. Yang, Y. Zhong, M. Qian, C. Li, Z. Zhang, G. Xing, S. Huettner, Y. Tao, Y. Li, W. Huang, *npj Flexible Electron.* **2018**, *2*, 1.
[15] M. K. Kim, T. Jeon, H. I. Park, J. M. Lee, S. A. Nam, S. O. Kim, *CrystEngComm* **2016**, *18*, 6090.
[16] C. Bi, Q. Wang, Y. Shao, Y. Yuan, Z. Xiao, J. Huang, *Nat. Commun.* **2015**, *7*, 6.
[17] Z. Liang, S. Zhang, X. Xu, N. Wang, J. Wang, X. Wang, Z. Bi, G. Xu, N. Yuan, J. Ding, *RSC Adv.* **2015**, *5*, 60562.
[18] X. Y. Chin, D. Turkay, J. A. Steele, S. Tabean, S. Eswara, M. Mensi, P. Fiala, C. M. Wolff, A. Paracchino, K. Artuk, D. Jacobs, Q. Guesnay, F. Sahli, G. Andreatta, M. Boccard, Q. Jeangros, C. Ballif, *Science* **2023**, *381*, 59.
[19] X. Luo, H. Luo, H. Li, R. Xia, X. Zheng, Z. Huang, Z. Liu, H. Gao, X. Zhang, S. Li, Z. Feng, Y. Chen, H. Tan, *Adv. Mater.* **2023**, *35*, 2207883.
[20] S. Shao, M. A. Loi, *Adv. Mater. Interfaces* **2020**, *7*, 1901469.
[21] M. Kim, G.-H. Kim, T. K. Lee, I. W. Choi, H. W. Choi, Y. Jo, Y. J. Yoon, J. W. Kim, J. Lee, D. Huh, H. Lee, S. K. Kwak, J. Y. Kim, D. S. Kim, *Joule* **2019**, *3*, 2179.
[22] J. Park, J. Kim, H. S. Yun, M. J. Paik, E. Noh, H. J. Mun, M. G. Kim, T. J. Shin, S. I. Seok, *Nature* **2023**, *2*, 1.
[23] X. Liu, Y. Guo, Y. Cheng, S. Lu, R. Li, J. Chen, *Chem. Commun.* **2023**, *59*, 13394.
[24] C. Pereyra, H. Xie, M. Lira-Cantu, *J. Energy Chem.* **2021**, *60*, 599.
[25] K. Odysseas Kosmatos, L. Theofylaktos, E. Giannakaki, D. Deligiannis, M. Konstantakou, T. Stergiopoulos, *Energy Environ. Mater.* **2019**, *2*, 79.
[26] H. Bazzazzadegan, Y. Mortazavi, A. Khodadadi, M. Mohagheghian, *Superlattices Microstruct.* **2018**, *123*, 218.
[27] T. Xu, X. Sun, W. Cao, X. Qin, A. Gurung, S. Lv, Y. Chen, L. Chen, W. Huang, Q. Qiao, *ChemNanoMat* **2020**, *6*, 806.
[28] L. Han, S. Cong, H. Yang, Y. Lou, H. Wang, J. Huang, J. Zhu, Y. Wu, Q. Chen, B. Zhang, L. Zhang, G. Zou, *Sol. RRL* **2018**, *2*, 1800054.
[29] X. Wen, Q. Cai, G. Shen, X. Xu, P. Dong, Y. Du, H. Dong, C. Mu, *Nanotechnology* **2021**, *32*, 30LT02.
[30] O. Er-Raji, L. Rustam, B. P. Kore, S. W. Glunz, P. S. C. Schulze, *ACS Appl. Energy Mater.* **2023**, *6*, 6183.
[31] M. M. Tavakoli, M. Saliba, P. Yadav, P. Holzhey, A. Hagfeldt, S. M. Zakeeruddin, M. Grätzel, *Adv. Energy Mater.* **2019**, *9*, 1802646.
[32] M. M. Byranvand, M. Saliba, *Sol. RRL* **2021**, *5*, 2100295.
[33] H. H. Wills, *Proc. R. Soc. London, Ser. A* **1965**, *284*, 272.
[34] O. Er-raji, M. A. A. Mahmoud, O. Fischer, A. J. Ramadan, D. Bogachuk, A. Reinholdt, A. Schmitt, B. P. Kore, T. W. Gries, A. Musiienko, O. Schultz-Wittman, M. Bivour, M. Hermle, M. C. Schubert, J. Borchert, S. W. Glunz, P. S. C. Schulze, *Joule* **2024**, *7*, 1.

[35] J. H. Hollomon, D. Turnbull, *Prog. Met. Phys.* **1953**, *4*, 333.
[36] M. R. Shedam, A. Venkateswara Rao, *Mater. Chem. Phys.* **1998**, *52*, 263.
[37] N. Karpukhina, R. G. Hill, R. V. Law, *Chem. Soc. Rev.* **2014**, *43*, 2174.
[38] F. Hou, *Commun. Chem.* **2021**, *4*, 1.
[39] W. Li, G. Yu, S. Wang, J. Ding, X. Xu, Q. Gu, D. Wang, P. Huang, *RSC Adv.* **2017**, *7*, 17531.